HHS Public Access

Author manuscript

Nature. Author manuscript; available in PMC 2023 January 06.

Published in final edited form as:

Nature. 2022 July ; 607(7919): 534–539. doi:10.1038/s41586-022-04923-7.

A receptor-channel trio conducts Ca^{2+} signaling for pollen tube reception

Qifei Gao[1], **Chao Wang**[1], **Yasheng Xi**[1], **Qiaolin Shao**[1], **Legong Li**[2], **Sheng Luan**[1,*]

[1]Department of Plant and Microbial Biology, University of California at Berkeley; Berkeley, CA, 94720, USA

[2]College of Life Sciences, Capital Normal University; Beijing, 100048, China

Abstract

Precise signaling between pollen tubes and synergid cells in the ovule initiates fertilization in flowering plants[1]. The arrival of pollen tube to the ovule triggers Ca^{2+} spiking in the synergids[2,3] that induce pollen tube rupture and sperm release. This process, named pollen tube reception, entails action of three synergid-expressed genes in *Arabidopsis*, including *FERONIA* (*FER*) encoding a receptor-like kinase (RLK), *LORELEI* (*LRE*) for a glycosylphosphatidylinositol (GPI)-anchored protein, and *NORTIA* (*NTA*) for a transmembrane protein of unknown function[4–6]. While genetic analyses have placed these three players in the same pathway, it remains unknown how they work together to enable synergid-pollen tube communication. We identified two pollen-tube-derived small peptides[7] of the rapid alkalinization factor (RALF) family[8] as ligands for the FER-LRE co-receptor that in turn recruited NTA to the plasma membrane. We revealed that NTA functioned as a calmodulin-gated Ca^{2+} channel required for calcium spiking in the synergid. We further reconstituted the biochemical pathway in which FER-LRE perceived pollen tube-derived peptides to activate the NTA calcium channel and initiate calcium spiking, a second messenger for pollen tube reception. The FER-LRE-NTA trio thus formed a previously unanticipated receptor-channel complex in the female cell to recognize male signals and trigger fertilization process.

As a ubiquitous second messenger, Ca^{2+} regulates many aspects of physiology and development in both animals and plants[9–11]_ENREF_9_ENREF_8, including reproduction. In animals, Ca^{2+} signals drive the motility of sperms[12] and forecast the successful

*Correspondence and requests for materials should be addressed to S. L., sluan@berkeley.edu.

Author contributions:

Q.G., C.W., L.L., and S.L. conceived and designed the experiments; Q.G., Y.X. and Q. S. performed molecular cloning, transgenic plant, and biochemical experiments; Q.G. performed patch-clamp and voltage clamp recordings and Ca^{2+} imaging. All experiments were independently reproduced in the laboratory. Q.G., C.W. and S.L. wrote the manuscript. All authors discussed the results and commented on the manuscript.

Competing interests: Authors declare that they have no competing interests.

Reporting summary

Further information on research design is available in the Nature Research Reporting Summary linked to this paper.

Additional information

Supplementary Fig. 1

This file contains uncropped gel images of Fig. 1a, 1b, 1c and 2c with size markers.

Supplementary information Videos 1 to 10

fertilization[13]. In flowering plants, sperms are immobile and require a special delivery structure called pollen tube that navigates in the female tissues and finds the ovule before releasing sperms[1]. From pollen germination, pollen tube guidance, to pollen tube reception, each step of the way requires intricate Ca^{2+} signaling[14]. However, the molecular mechanism underlying calcium signaling in plant reproduction remains largely unknown. During pollen tube reception, interaction between pollen tube and synergids in the ovule activates Ca^{2+} oscillations in both partners, leading to pollen tube burst and synergid cell death and initiating fertilization[2,3,15,16]_ENREF_3. On the female side, FER, LRE, and NTA are three components in the same pathway required for synergid Ca^{2+} spiking in response to pollen tube arrival, but little is known on how they work together to mediate Ca^{2+} entry. We show here that pollen tube RALFs bind to FER-LRE coreceptors that recruit NTA, a calcium channel, to form a receptor-channel assembly. This tri-molecular complex is regulated by Ca^{2+}-calmodulin-dependent feedback inhibition, driving Ca^{2+} oscillations in the synergid.

RALFs Trigger Synergid Ca^{2+} Oscillation

FER and LRE are both required for pollen tube reception and may function as a co-receptor for unknown signals derived from pollen tube[4,5,17–20]. We hypothesized that such signals may be RALF family peptides because some RALFs bind to either FER alone[21,22] or both FER and LRE-like proteins (LLGs) in other processes[23–25]_ENREF_9. Among the 37 *Arabidopsis* RALFs, at least 8 of them, including RALF4, 8, 9, 15, 19, 25, 26 and 30, are expressed in pollen tubes[7]. We expressed and purified the 8 pollen tube-derived RALF peptides and examined their interaction with FER[23]. We also included in the assay an ovule derived RALF peptide (RALF34) that is closely related to pollen tube RALFs such as RALF4 and 19. The extracellular domain of FER pulled down RALF4, RALF19 and RALF34 (Fig.1a, Supplementary Fig. 1a). Consistent with this result, RALF4 and 19 were found to act antagonistically with RALF34 through interaction with the same receptors of the FER family for pollen tube integrity[7].

As ligands for FER-LLGs co-receptor, RALFs enhance interaction between FER and LLGs[23]. Consistent with this model, we found that RALF4/19/34 enhanced the interaction between GST-LRE and MBP-FER_{ex}, whereas several other RALFs did not (Fig.1b lower panel, Supplementary Fig. 1b). This observation was confirmed by co-immunoprecipitation (Co-IP) assay with total proteins from *Nicotiana benthamiana* leaf tissue expressing LRE-Myc and FERK565R-Flag (Fig.1c, Supplementary Fig. 1c). RALF4 was reported to be secreted into the apoplast of pollen tube[26], and our promoter-GUS (β-glucuronidase) analysis confirmed expression of RALF4 and RALF19 during pollen tube reception (Extended Data Fig. 1a), making it feasible for RALF4 and RALF19 to interact with FER and LRE in the synergid. Together, these results suggested that FER-LRE may function as co-receptors for pollen tube RALFs, including RALF4 and RALF19.

In response to pollen tube arrival, the synergids produce specific Ca^{2+} fluctuations required for pollen tube reception[2,3]. If RALFs signal pollen tube arrival, they should produce a similar Ca^{2+} entry in the synergids when applied to isolated ovules *in vitro*. We generated transgenic plants expressing Ca^{2+} indicator GCaMP6s[27] driven by a synergid-specific promoter (p*MYB98*)[28] and examined $[Ca^{2+}]_{cyt}$ changes in the synergids in response to

RALFs. In the wild type (WT) synergids, RALF4 and 19, but not RALF34, induced $[Ca^{2+}]_{cyt}$ elevations (Fig.1d and i; Supplementary Video 1, 2, and 3), consistent with the idea that RALF34 binds to the same receptors but function differently[7]. Several other pollen tube RALFs (8, 9, 15, 25, 26 and 30) that did not bind FER also failed to induce synergid $[Ca^{2+}]_{cyt}$ changes (Extended Data Fig. 2). In the pollen tube reception assay, the receptive synergid and nonreceptive synergid in one ovule showed distinct calcium spikes[2]. However, we found that exogenous RALF4/19 induced similar Ca^{2+} transients in both synergid cells in one ovule, suggesting that RALFs in the solution may have diffused evenly towards the two synergids, whereas pollen tube positions itself closer to one of the two synergids leading to asymmetrical signaling.

We then examined pollen tube-triggered synergid Ca^{2+} changes[2,3] and compared with those induced by RALFs. As reported earlier[3], synergid Ca^{2+} dynamics followed three phases as pollen tube progresses to reception: (I) $[Ca^{2+}]_{cyt}$ oscillates at a regular pace when pollen tube enters the micropyle and approaches the synergid; (II) $[Ca^{2+}]_{cyt}$ sustained at a higher level after pollen tube penetrates the synergid; (III) $[Ca^{2+}]_{cyt}$ goes down when synergid collapses. The amplitude and periodicity of RALF4/19-triggered Ca^{2+} oscillations were similar to the phase I of the pollen tube-induced Ca^{2+} spiking (Fig.1d–i and Extended Data Fig. 3, and Supplementary Video 4), suggesting that pollen tube derived RALF4/19 mimic the early phase of pollen tube arrival before mechanical penetration.

We then tested if RALF4 and 19 induced such Ca^{2+} spiking in a FER-LRE-dependent manner. Indeed, synergids from *fer-4* and *lre-5* mutants failed to respond to RALF4, RALF19, or pollen tube arrival[3] (Fig.1, e, f and i; Extended Data Fig. 3; Supplementary Video 5 and 6). In addition to *fer* and *lre* mutants, the mutant lacking NORTIA (NTA) was non-responsive to 0.5 μM RALFs although a portion of *nta-3* synergid showed weaker responses to an elevated level of RALFs (2 μM) in the Ca^{2+} imaging assay (Fig.1, g and i; Extended Data Fig. 3; Supplementary Video 7). Comparing with *fer* and *lre* mutant, the weaker defect in *nta-3* may suggest a partial functional redundancy with another NTA-like component.

MLO Proteins Are Ca^{2+} Channels

The NTA protein is a member of the MILDEW RESISTANCE LOCUS O (MLO) protein family[6]. Originally discovered as a genetic determinant for powdery mildew resistance in barley[29], the MLO proteins feature multi-transmembrane domains and a calmodulin-binding domain (CaMBD)[30,31]. *Arabidopsis* genome encodes 15 MLO proteins (named *At*MLO1–15) some of which are functionally linked to root thigmomorphogenesis[32], powdery mildew susceptibility[33], and pollen tube growth[34]. NTA (*At*MLO7) is specifically expressed in synergids and appears to function downstream of FER-LRE module in pollen tube reception[6]. The biochemical function of MLOs remains unknown, representing a critical gap of knowledge on the signaling pathways in which they participate[31]. In the case of NTA, genetic analysis indicates that it works together with FER-LRE co-receptors in the same pathway to induce Ca^{2+} influx. Because NTA and other MLOs are multi-transmembrane proteins, we hypothesized that NTA could be one of the missing Ca^{2+} transporting proteins responsible for synergid Ca^{2+} entry.

To test whether MLO proteins transport Ca^{2+}, we performed a Ca^{2+} transport assay with all 15 MLO members from *Arabidopsis*, the barley MLO (*Hv*MLO), and 2 MLO members from *Physcomitrella patens*, which represent dicot, monocot, and basal land plant MLOs, respectively. In single-cell Ca^{2+} imaging assay[35], we found that *At*MLO2, 3, 4, 10, 12, *Hv*MLO, *Pp*MLO2 and *Pp*MLO3 mediated Ca^{2+} entry when expressed in COS7 cells (Fig.2a and Extended Data Fig. 4). To confirm Ca^{2+} imaging results, we used patch-clamp to directly measure transport activity of *At*MLO2 and recorded large inward currents that depended on external Ca^{2+} concentrations (Extended Data Fig. 5, a and b). We also found that *At*MLO2 was permeable to Ba^{2+} and Mg^{2+}, but not to K^+ or Na^+ (Extended Data Fig. 5, c, d, e, f, i, j, k and l). Furthermore, two typical Ca^{2+} channel blockers lanthanum (La^{3+}) and gadolinium (Gd^{3+}) inhibited the *At*MLO2-mediated inward currents (Extended Data Fig. 5, g and h). Like *At*MLO2, *Hv*MLO also mediated Ca^{2+} influx (Extended Data Fig. 6). These results indicate that MLO proteins function as Ca^{2+}-permeable channels.

FER-LRE-NTA Trio Mediates Ca^{2+} Entry

Many of the tested MLOs (including NTA) failed to mediate Ca^{2+} entry in the HEK293T or COS7 cells (Fig.2a and Extended Data Fig. 4; Supplementary Video 8 and 9). We speculated that they may require other components to be active or they may not be properly targeted to plasma membrane (PM). Indeed, NTA mainly accumulates in a Golgi-associated compartment[36] and relocates to the synergid filiform apparatus in a FER and LRE dependent manner[6,37]. In our Ca^{2+} transport assays, PM localization was critical for mediating Ca^{2+} entry if NTA was indeed a Ca^{2+} channel. We found that NTA-GFP was largely localized to the intracellular punctate structures in the COS7 cells (Fig. 2b). When co-expressed with FER and LRE, however, NTA-GFP was targeted to the PM (Fig. 2b). Such PM targeting was not achieved by co-expressing NTA-GFP with either FER or LRE alone, consistent with the finding that LRE/LLG1 physically interacts with and chaperones FER to the PM[19] and FER was required for the redistribution of NTA to the PM[6]. We further showed that NTA directly interacted with FER and LRE enhanced such interaction (Fig.2c, Supplementary Fig. 1d), indicating that FER, LRE and NTA form a complex we referred to as NTA trio.

As FER and LRE together targeted NTA to the PM, we tested if NTA trio would produce a functional channel at the PM. Co-expressing with FER and LRE in the COS7 cells enabled NTA to mediate Ca^{2+} influx in both the imaging assay and patch-clamp recording (Fig.2d, Supplementary Video 10 and Extended Data Fig.7). Like *At*MLO2 and *Hv*MLO, NTA trio also conducted currents carried by divalent cations (Ca^{2+}, Ba^{2+} and Mg^{2+}), but not monovalent cations (K^+ and Na^+) (Extended Data Fig. 8). The Ca^{2+} channel activity of NTA trio was inhibited by La^{3+} and Gd^{3+} that also blocked synergid Ca^{2+} spiking (Extended Data Fig. 8). The kinase-dead version of FER also formed active NTA trio (Fig.2, d, g and h), consistent with the earlier finding that the kinase activity of FER was not required for pollen tube reception[38,39].

Our data suggested that NTA is an active Ca^{2+} channel but requires FER-LRE for targeting to the PM. We tested this idea by constructing a PM-localized chimeric NTA-MLO1 protein[36,37] and found that NTA-MLO1 mediated Ca^{2+} influx independently from FER-LRE (Fig.2, j–m).

RALFs Enhance FER-LRE-NTA Activity

We then tested the effect of RALFs on the NTA trio activity and found that RALF4/19, but not RALF34, significantly enhanced the Ca^{2+} channel activity of the NTA trio (Fig.3, a, b, c and d), consistent with the finding that RALF4/19 strongly induced synergid Ca^{2+} elevation (Fig.1, d and e). We further confirmed this observation by reconstitution of RALFs-FER-LRE-NTA pathway in *Xenopus* oocytes and monitoring channel activity via two electrode voltage-clamp (TEVC) (Fig.3, e and f). The chimeric NTA-MLO1 co-expressed with FER and LRE was also enhanced by RALF4/19, but not by RALF34 (Fig.3, g, h, i and j). Concerning the mechanism underlying RALF4/19-dependent activation of the channel, a previous study showed that NTA is redistributed to the filiform apparatus of synergid upon pollen tube arrival[6]. We examined the PM localization of NTA in response to RALFs but failed to observe any discernible effect of RALF4/19 application (Extended Data Fig. 9a). In this mammalian cell system, FER and LRE clearly facilitated the PM localization of NTA (Fig.2b), implying that a portion of NTA can be localized in the PM of synergid in a pollen-tube-independent manner. Upon pollen tube arrival, RALF4/19 and possibly other pollen-tube signals (e.g., mechanical stimulus) may further activate the Ca^{2+} channel by recruiting the trio to a specific locus (filiform apparatus).

During the revision of this manuscript, five other pollen tube RALFs (RALF6, 7, 16, 36, and 37) were reported to bind FER, ANJEA (ANJ), and HERCULES RECEPTOR KINASE 1 (HERK1) and function redundantly in polytubey block and pollen tube reception[40]. We analyzed RALF37 in our assays and found that RALF37, like RALF4/19, also triggered synergid Ca^{2+} changes and activated the NTA trio (Extended Data Fig.10). This result suggested that multiple RALFs derived from pollen tube serve as signals in triggering synergid calcium spiking, leading to pollen tube reception, consistent with our observation that *ralf4* and *ralf19* single mutants showed no detectable phenotypic defects (Extended Data Fig. 1b and c).

NTA-CaM Shapes Synergid Ca^{2+} Spiking

MLO proteins feature a CaMBD in the intracellular C-terminal region[30,31], suggesting that MLOs may be regulated by CaM-binding, a typical auto-regulatory mechanism for many Ca^{2+}-channels in both animal and plant systems[41,42]. We examined how CaM may affect the channel activity of MLO proteins by co-expressing CaM7 with NTA trio or other MLOs including *At*MLO2, *Hv*MLO, and NTA-MLO1 in the COS7 cells. A dramatic inhibition of Ca^{2+} entry was observed in all cases (Fig.4, a and b), revealing an inhibitory feedback of MLO channel activity by CaM. We confirmed this mechanism by showing that a mutant NTA (named as NTA^{RR}) in which Leu455 and Trp458 were mutated to Arg to abolish its CaM-binding[37] failed to respond to CaM-mediated inhibition (Fig.4, a and b). Although these mutations in CaMBD partially impaired NTA's redistribution to the filiform apparatus in the synergid[37], we found that NTA^{RR} trio was recruited to the PM in the COS7 cell (Extended Data Fig. 9b), consistent with the finding that NTA^{RR} trio still conducted Ca^{2+} entry.

As CaM binds to *Hv*MLO in a Ca^{2+} dependent manner[43], we proposed that CaM may inhibit NTA channel activity upon elevation of cytosolic Ca^{2+} levels as a negative feedback. We tested this hypothesis by titration of cytosolic Ca^{2+} levels and expressing CaM7 mutant lacking Ca^{2+} binding EF hands[44]. Our results showed that CaM7 requires Ca^{2+} binding to inhibit NTA trio activity (Fig.4, c, d and g). Likewise, the NTA mutant defective in CaM binding (NTA^{RR}) became constitutively active (Fig.4, e, f and g). These results support a model in which RALFs activate NTA channel to elevate synergid $[Ca^{2+}]_{cyt}$ to a threshold level that in turn enables CaM binding and inhibition of the NTA channel activity.

Specific Ca^{2+} spiking in synergids is essential for pollen tube reception[2,3]. We hypothesized that Ca^{2+}-CaM-dependent feedback inhibition of NTA channel provides a mechanism for shaping such a Ca^{2+} signature. To test this idea *in planta*, we generated transgenic plants harboring NTA^{RR} mutant driven by *NTA* promoter in the *nta-3* mutant background and examined synergid $[Ca^{2+}]_{cyt}$ spikes in response to RALF4. We found that $[Ca^{2+}]_{cyt}$ spiking in the synergids was exaggerated in NTA^{RR} plants (Fig.4, h–k). We also observed higher levels of Ca^{2+} elevation in NTA^{RR} synergid in response to pollen tube arrival and a disordered oscillation pattern as compared to WT (Fig.4, j and k). This result indicated that NTA^{RR} lacking CaM-dependent inhibition produced a sustained increase in $[Ca^{2+}]_{cyt}$, causing defect in pollen tube reception[37].

Conclusions

We have identified pollen tube-derived RALF peptides as ligands for FER-LRE co-receptor complex that recruits NTA, a CaM-gated Ca^{2+} channel, to the plasma membrane domains to initiate Ca^{2+} entry and pollen tube reception (Fig.4, l). This work has thus demonstrated a mechanistic process integrating the action of FER, LRE, and NTA, the three players genetically connected in synergid-pollen tube interaction. In addition, identifying MLO proteins as Ca^{2+} channels uncovered the long sought-after common biochemical pathway (calcium entry) that entails MLO functions in multiple physiological processes, including but may not be limited to mildew resistance, root mechano-sensing, pollen tube growth, and fertilization in plants. Indeed, calcium is a core component in all these processes[11,14] and our finding here set the stage for extensive future research to address mechanisms in various MLO-dependent processes. Since FER-LRE/LLG co-receptors are often connected to calcium spikings in other signaling processes beyond reproduction[21], identifying a MLO channel downstream the FER/LRE co-receptors may offer a possible mechanism for other RALF-FER/LLG-dependent pathways. In the context of calcium signaling, a common theme in all eukaryotes, MLOs represent a family of calcium channels unique to plant kingdom, suggesting that, instead of having fewer calcium channels than animals as thought in the current dogma[11], plants may feature channels distinct from animal counterparts and more of these novel channels await to be discovered.

In the context of reproduction, our study raised several important questions for future research into mechanistic details of male-female interaction. For example, while RALF4/19 bind to FER/LRE and enhance the channel activity of NTA, the mechanism underlying this activation awaits to be resolved by structural analysis of the FER/LRE/NTA trio in the presence of the RALF ligands. Prior to the pollen tube reception, pollen tube integrity

and guidance also involve the function of several RALF peptides, FER family RLKs, and MLOs. Our study may provide a strategy for further research to link these components in distinct Ca^{2+} signaling pathways. A previous report noted that MLO5/9 may be trafficked together with cyclic nucleotide-gated channel 18 (CNGC18), another calcium channel with an essential role in pollen tube growth and guidance[34]. This raises an interesting question that concerns the functional interplay of multiple calcium channels in shaping specific calcium signatures in pollen tube, synergid and other cell types in plants[42].

Methods

Plant materials and growth conditions

Seeds were sterilized with 10% (v/v) bleach and sown on agar plates containing 1/2 MS medium (1/2 MS, 0.8% [w/v] Phyto agar, and 1% [w/v] sucrose, pH adjusted to 5.8 with KOH). Plates were incubated at 4°C for 3 days for stratification and then transferred to the soil pots in 22°C growth room with a 16-hour light/8-hour dark cycle (100 μmol m^{-2} s^{-1}). The seeds for *fer-4* (GABI_GK106A06), *lre-5* (CS66102) and *nta-3* (SALK_027128) were purchased from *Arabidopsis* Biological Resource Center (ABRC). The *ralf4* and *ralf19* mutants were generated by CRISPR as reported[7].

Transgenic plants

The coding DNA sequence (CDS) of GCaMP6s was PCR-amplified using HBT-GCaMP6-HA as template[27] and fused to the *MYB98* promoter region[28] amplified from Columbia-0 (Col-0) genomic DNA in the pCAMBIA 2300 vector. The binary construct was transformed into *Arabidopsis thaliana* (Col-0) plants via *Agrobacterium* (GV3101) using the floral dip method[45]. Transgenic plants were selected on 1/2 MS plates containing 50 mg/L kanamycin, and one homozygous transgenic p*MYB98-GCaMP6s* line was then crossed with *fer-4*, *lre-5* and *nta-3* and further brought to homozygosity concerning both GCaMP6s and *fer-4*/*lre-5*/*nta-3* genetic background. The NTA^{RR} mutant version was produced by site-directed mutagenesis to replace Leu455 and Trp458 with Arg. The *NTA* promoter region was PCR-amplified from Col-0 genomic DNA and fused with NTA^{RR} CDS in the pCAMBIA 1305 vector and transformed into plants as described above.

GUS staining

The mature pistils of the transgenic plants carrying pro*RALF4*/*19*: GUS were dissected to isolate intact ovules that were then fixed in 80% acetone overnight and incubated in the GUS staining buffer consisting of 50 mM sodium phosphate, pH 7.2, 2 mM potassium ferrocyanide, 2 mM potassium ferricyanide, 0.2% Triton X-100, and 2 mM X-Gluc. Images were taken using the Zeiss AxioObserver Z1 Inverted Microscope.

Aniline blue staining

Pollen grains of the freshly opened flower of wild type or mutant lines were used to pollinate the WT pistils that had been emasculated one day earlier. After 24 hours, the pistils were fixed in acetic acid/ethanol

1:3 overnight. They were then washed stepwise by 70% ethanol, 50% ethanol, 20% ethanol, and ddH_2O. The pistils were treated with 8 M NaOH overnight to soften the tissues and then washed with ddH_2O for three times before staining with aniline blue solution (0.1% aniline blue, 50 mM K_3PO_4) for 2 hours. The stained pistils were observed under the Zeiss AxioObserver Z1 Inverted Microscope.

Mammalian cell culture, vector construction, and transfection

The CDS of GCaMP6s was amplified from HBT-GCaMP6-HA[27] and cloned into a dual-promoter vector, pBudCE4.1 (Invitrogen), with each CDS for NTA, FER, LRE, NTA-MLO1 for co-expression in HEK293T or COS7 cell. The chimeric NTA-MLO1 CDS was generated as published[36].

Mammalian cells were cultured in Dulbecco's Modified Eagle's Medium (DMEM) supplemented with 10% fetal bovine serum in a 5% CO_2 incubator at 37°C with controlled moisture. HEK293T or COS7 cells were transfected using Lipofectamine™ 3000 Transfection Reagent Kit (Invitrogen). Plasmids for transfection were extracted from *E. coli* (DH5α) using QIAGEN Plasmid Mini Kit (Qiagen), and 2 μg plasmid DNA was added into each well of 6-well plates (Nunc) containing the cells (70–80% confluent). To confirm that the cells were successfully transfected, green and/or red fluorescent signals were examined using an inverted fluorescence microscope (Zeiss AxioObserver Z1 Inverted Microscope) before patch clamp and Ca^{2+} imaging experiments 48 hours after transfection.

Whole-cell patch-clamp recording

The whole-cell patch-clamp experiments were performed using an Axopatch-200B patch-clamp setup (Axon Instruments, CA, USA) with a Digitata1550 digitizer (Axon Instruments, CA, USA) as previously described[46]. Clampex10.7 software (Axon Instruments, CA, USA) was used for data acquisition and Clampfit 10.7 was used for data analysis.

To record Ca^{2+} currents across the plasma membrane of HEK293T cells, the standard bath solution contained 140 mM N-Methyl-D-Glucamine (NMDG)-Cl, 10 mM $CaCl_2$, 10 mM glucose, and 10 mM Hepes, adjusted to pH 7.2 with $Ca(OH)_2$. The standard pipette solution contained 140 mM Cs-glutamate, 6.7 mM EGTA, 3.35 mM $CaCl_2$, and 10 mM Hepes, adjusted to pH 7.2 with CsOH. Free [Ca^{2+}] in the pipette solution was 175 nM, as calculated using the Webmaxc Standard (web.stanford.edu/~cpatton/webmaxc/webmaxcS.htm). The 10 mM Ca^{2+} in the bath solution was removed to attain 0 mM Ca^{2+} or substituted with 10 mM Ba^{2+} or 10 mM Mg^{2+} as indicated. A ramp voltage protocol of 2-second-duration from −160 mV to +30 mV (holding potential 0 mV) was applied 1 minute after accessing to a whole-cell configuration, and currents were recorded every 20 seconds for 5 repeats in total for each cell. The 5 current traces were used for statistical analysis for average current-voltage curves.

For inward K^+ current recordings in HEK293T cells, the bath solution contained 140 mM NMDG-Cl, 14.5 mM KCl, 10 mM glucose, and 10 mM Hepes, adjusted to pH 7.2 with KOH. The pipette solution contained 145 mM K-glutamate, 3.35 mM EGTA, 1.675 mM $CaCl_2$, and 10 mM Hepes, adjusted to pH 7.2 with KOH. The free Ca^{2+} concentration in the pipette solution was 100 nM, as calculated using the Webmaxc Standard.

For inward Na^+ current recordings in HEK293T cells, the bath solution contained 140 mM NaCl, 10 mM glucose, and 10 mM Hepes, adjusted to pH 7.2 with NaOH. The pipette solution contained 135 mM CsCl, 10 mM NaCl, 3.35 mM EGTA, 1.675 mM $CaCl_2$, and 10 mM Hepes, adjusted to pH 7.2 with CsOH. The free Ca^{2+} concentration in the pipette solution was 100 nM, as calculated using the Webmaxc Standard.

A step voltage protocol of 4-second-duration for each voltage from −160 mV to +60 mV with a +20 mV increment was used for K^+ and Na^+ current recordings in HEK293T cells 1 min after accessing to a whole-cell configuration.

TEVC recording from *Xenopus* oocytes

The CDS for NTA-3xHA, LRE-4xMyc and FER-3xFlag were cloned into the pGEMHE *Xenopus* oocyte expression vector. To construct LRE-4xMyc, the 4xMyc tag sequence was inserted after the first 60 bp of the LRE CDS encoding the signal peptide, followed by the downstream 438 bp of LRE as described previously[23].

The TEVC was performed as previously reported[35,44]. The capped RNA (cRNA) was synthesized from 1 μg of linearized plasmid DNA template using the mMESSAGE mMACHINE T7 kit (Ambion) and 10 ng of each cRNA, in a total volume of 46 nl, was injected into each oocyte. Injected oocytes were incubated in ND96 solution (96 mM NaCl, 2 mM KCl, 1 mM $MgCl_2$, 1.8 mM $CaCl_2$, 10 mM HEPES/NaOH, pH 7.4) at 18 °C for 2 days before electrophysiological recording. Oocytes were voltage-clamped using a TEV 200A amplifier (Dagan), a Digidata 1550 A/D converter, and recorded by CLAMPex 10.7 software (Axon Instruments). The pipette solution contained 3 M KCl. The standard bath solution contained 30 mM $CaCl_2$, 1 mM KCl, 2 mM NaCl, 130 mM mannitol and 5 mM MES-Tris (pH 5.5). Voltage steps were applied from +40 to−160 mV in −20 mV decrements during 0.8 s.

Single-cell Ca^{2+} imaging in mammalian cells

HEK293T or COS7 cells expressing GCaMP6s and various combinations of candidate channel proteins were monitored by a Zeiss AxioObserver Z1 Inverted Microscope (Ivision 4.5 software) using a 20 × objective as previously reported[35]. The interval of data acquisition was 2 seconds. The standard solution for Ca^{2+} imaging contained 120 mM NaCl, 3 mM KCl, 1 mM $MgCl_2$, 1.2 mM $NaHCO_3$, 10 mM Glucose, 10 mM HEPES, pH 7.5. About 60 seconds after initiation of imaging procedure, the bath was perfused using a peristaltic pump with the standard solution supplemented with 10 mM Ca^{2+} and/or RALFs to elicit Ca^{2+} entry through active channels.

Synergid cell Ca^{2+} imaging

For RALF induced synergid $[Ca^{2+}]_{cyt}$ elevation experiment, unfertilized ovules were dissected from flowers as reported[47]. The pistil was dissected to remove the ovules from the placenta using a surgical needle. The isolated ovules were placed in the pollen germination medium (PGM) containing 18% sucrose, 0.01% boric acid, 1mM $MgSO_4$, 1mM $CaCl_2$, 1mM $Ca(NO_3)_2$ and 0.5% agarose, pH7.0[48]. After 2-hour incubation at 22°C and 100% relative humidity, synergids expressing GCaMP6s were monitored by a Zeiss AxioObserver

Z1 Inverted Microscope (Ivision 4.5 software) using a 20 × objective, and various RALFs were added to the ovules as indicated.

For pollen tube induced synergid $[Ca^{2+}]_{cyt}$ elevation experiment, we followed the published protocol[2,3]. Dissected ovules of emasculated flowers expressing GCaMP6s were placed on the PGM. Unpollinated pistils were cut with a razor blade (VWR International, USA) at the junction between the style and ovary. The stigmas were placed on the PGM and manually pollinated with pollen grains expressing DsRed. Pollenated stigmas were positioned 150 μm away from the ovules and pollen tube growth was monitored under the fluorescence microscope. Time-lapse calcium imaging began after the pollen tube entered the ovule micropyle.

Protein Localization

Transfected COS7 cells were washed with phosphate-buffered saline (PBS), and mounted onto slides for image acquisition with a Zeiss LSM 880 confocal microscope and ZEN2012 software.

Peptide purification

All tag-free RALF peptides used in this study were purified from insect cells (High 5). The pFastBac vector containing RALF4, RALF19 and LRX8 were kind gifts from Julia Santiago of University of Lausanne, and RALF4/19 peptides were purified as reported[49].

For RALF8, 9, 15, 25, 26, 30 and 34, the CDS encoding RALF mature peptides were cloned into a modified pACEBAC1 (Geneva Biotech) vector in which RALFs were N-terminally fused to a 30 K signal peptide, a 10xHis tag, TRX A (Thioredoxin A) and a TEV (tobacco etch virus protease) site.

High 5 cells were infected with virus with a multiplicity of infection (MOI) of 3 and incubated for 1 d at 28 °C and 2 d at 22 °C at 110 rpm on an orbital shaker. The secreted peptides were purified from the supernatant by Ni^{2+} column (Ni-NTA, Qiagen), and incubated with TEV protease (New England Biolabs) to remove the tags. Peptides were further purified by size-exclusion chromatography on a Superdex 200 increase 10/300 GL column (GE Healthcare), equilibrated in 20 mM sodium citrate pH 5.0, 150 mM NaCl. The peptides were diluted with sterile pure water before use.

Protein–protein interaction assays

For pull-down assay, MBP-FER_{ex}, GST-RALFs, and GST-LRE were produced in *E. coli* Rosetta (DE3) by 0.1 mM IPTG induction overnight at 16 °C, and bound to amylose or glutathione resins for purification as reported[19,50]. The pull-down buffer contained 40 mM Tris–HCl, pH 7.5, 100 mM NaCl, 1 mM EDTA, 5% glycerol, 5 mM $MgCl_2$, 1 mM PMSF, cOmplete™ Protease Inhibitor Cocktail (Roche) at 1:100 dilution, and 0.4% Triton X-100. Proteins were applied to amylose resins and incubated at 4°C for 2 hours with gentle mixing. The resin was washed three times in pull-down buffer. Proteins remained bound to the resin were eluted by mixing with SDS/PAGE loading buffer, boiled for 5 min, and subjected to 12% SDS-PAGE and western blotting.

For co-IP in tobacco leaves, 35S:FERK565R-3xFlag and 35S:LRE-4Myc constructs were co-transformed into *Agrobacterium tumefaciens* (strain GV3101) and infiltrated into *Nicotiana benthamiana* leaves[23]. Sixty hours after inoculation, leaves were detached and treated with 5 μM RALFs for 2 hours before total protein was extracted and applied to ANTI-FLAG M2 Affinity Agarose Gel (Sigma-Aldrich). After incubation at 4°C for 2 hours with gentle mixing, the resin was washed three times in pull-down buffer, and the bound protein was eluted by mixing with SDS/PAGE loading buffer, boiled for 5 min, and subjected to 10% SDS-PAGE and western blotting.

For co-IP in *Xenopus* oocytes, cRNAs of FER-3xFlag, NTA-3HA and LRE-4Myc were injected into oocytes, incubated for 3 days, followed by treatment with 5 μM RALFs for 2 hours. Total protein was extracted in the pull-down buffer and then applied to ANTI-FLAG M2 Affinity Agarose Gel (Sigma-Aldrich). After incubation at 4°C for 2 hours with gentle mixing, the resin was washed three times in pull-down buffer, and the bound protein was eluted by mixing with SDS/PAGE loading buffer, boiled for 5 min, and subjected to 10% SDS-PAGE and western blotting.

For chemiluminescence detection, Anti-GST-HRP (1: 2 000 dilution), anti-Myc-HRP (1: 2 000 dilution), anti-HA (1: 2 000 dilution), anti-MBP (1: 2 000 dilution) and anti-mouse secondary (1:20 000 dilution) antibodies were from Santa Cruz Biotechnology, anti-Flag antibody (1: 4 000 dilution) was from Sigma-Aldrich.

Image processing and data analysis

Using the imageJ (1.51j8 version) software, GCaMP6s signals were analyzed overtime at several regions of interest (ROIs). To calculate the fractional fluorescence changes (ΔF/F), the equation $\Delta F/F = (F - F_0)/F_0$ was used, where F_0 denotes the average baseline fluorescence determined by the average of F over the first 10 frames of the recording before the treatment.

Microsoft Excel in office 365 and GraphPad Prism 7.0 were used for calculation and statistical analysis of the data; Adobe Illustrator CC 2019 was used for image assembly; Clampfit 10.7 was used to analyze and process data from electrophysiological experiments.

Extended Data

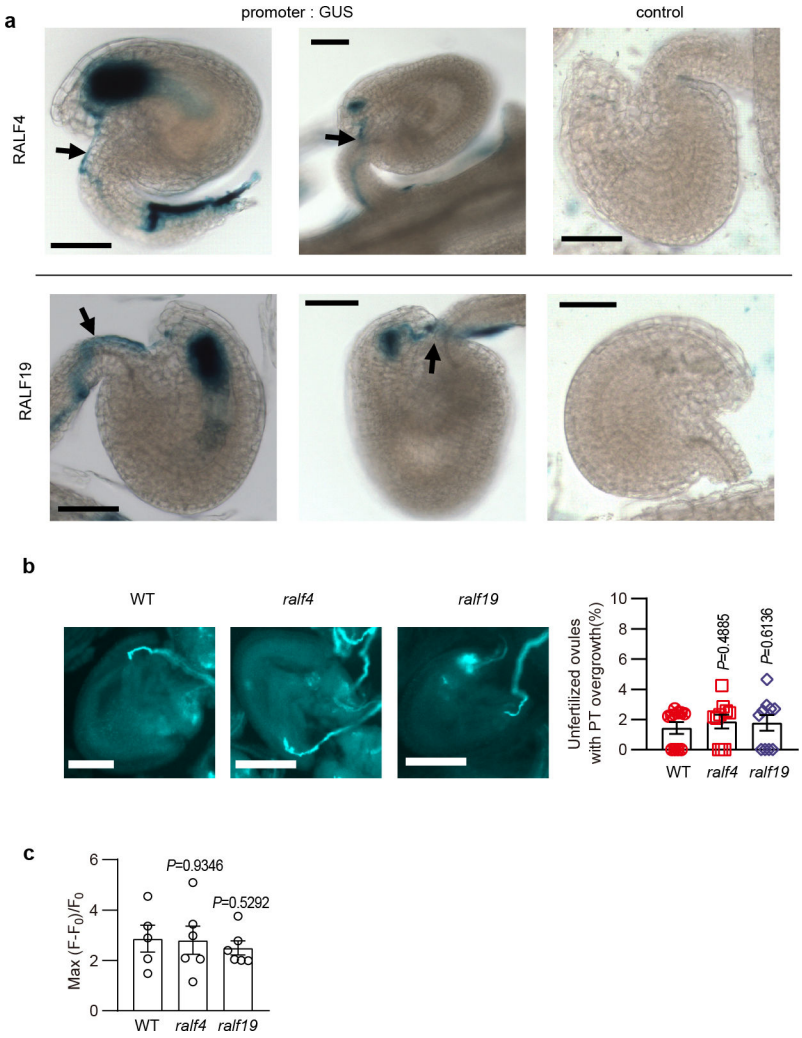

Extended Data Fig.1 |. Expression and redundant function of RALF4 and 19 in pollen tube reception.

a, Expression pattern of RALF4 and 19 during pollen tube reception. Arrows indicated pollen tubes (from pro*RALF*-GUS plants) that penetrated ovules (pro*RALF*-GUS plants). For control, pollen grains from non-transgenic plants were used to pollinate the promoter: GUS transgenic plants, showing no expression of GUS in the ovule. **b,** *ralf4* and *ralf19* single mutants did not show pollen tube overgrowth. n=10 pistils. **c,** The peak values of the synergid Ca^{2+} spikes triggered by pollen tubes of *ralf4* and *ralf19* single mutants was similar to that of WT. n=5 ovules for WT, and n=6 ovules for *ralf4* and *ralf19*. Bar, 50 μm. Error bars depict means ± S.E.M. All *P* values were determined by two-tailed Student's *t*-test.

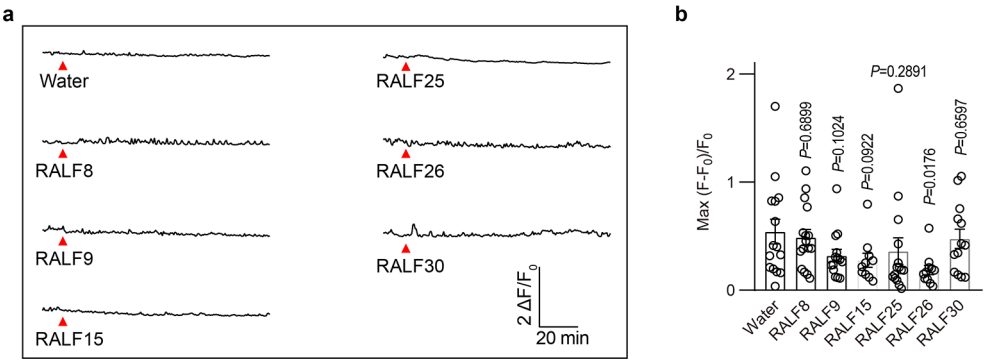

Extended Data Fig.2 |. RALF8, 9, 15, 25, 26 and 30 failed to induce synergid Ca^{2+} changes.
a, Representative Ca^{2+} spiking patterns in synergid cells in response to 0.5 μM RALFs. **b**, The peak values of Ca^{2+} spiking as in (**a**). n=15 ovules for water treatment, n=16 ovules for RALF8, n=14 ovules for RALF9, n=10 ovules for RALF15, n=15 ovules for RALF25, n=11 ovules for RALF26 and n=13 ovules for RALF30. Error bars depict means ± S.E.M. All *P* values were determined by two-tailed Student's *t*-test.

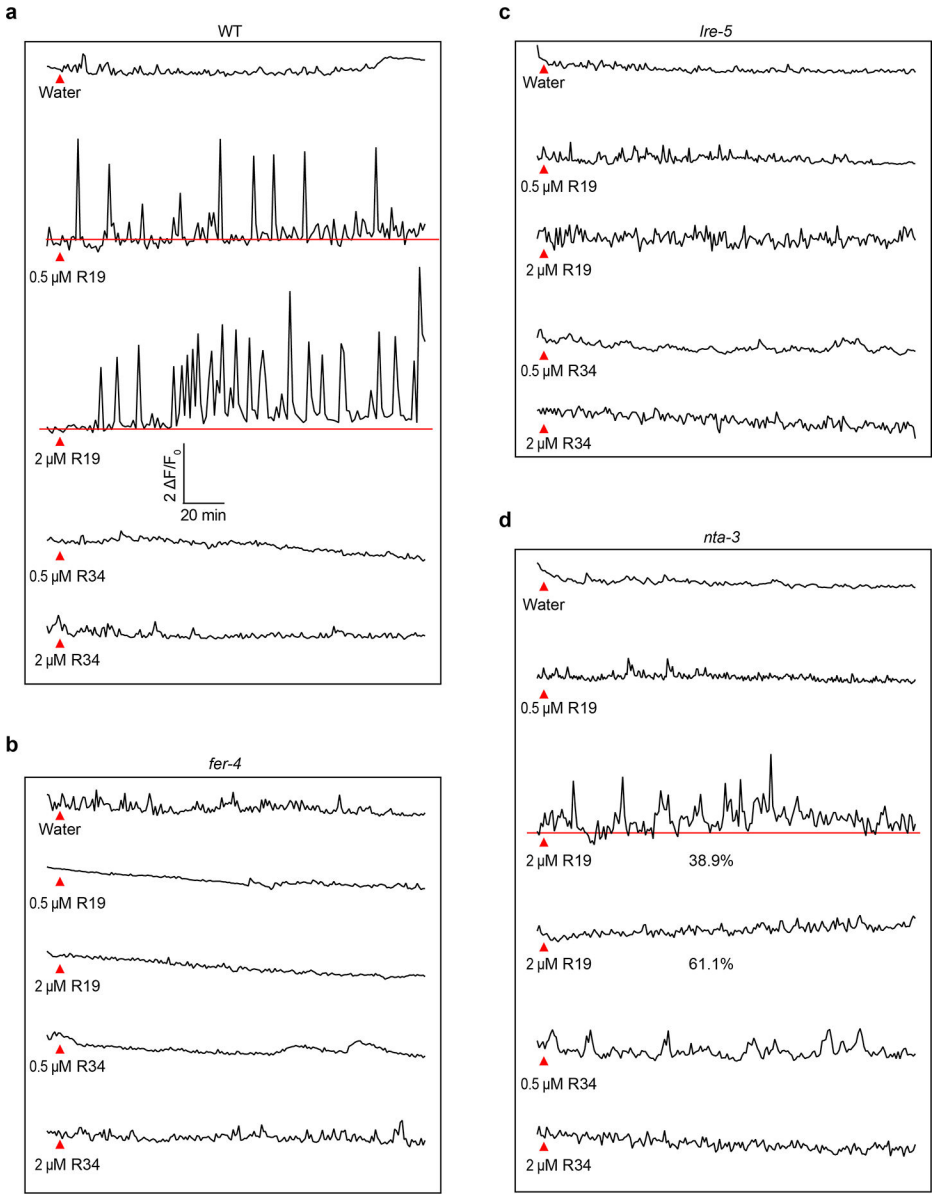

Extended Data Fig.3 |. Pollen tube derived RALF4/19 induce synergid Ca^{2+} oscillations.
Representative Ca^{2+} spiking patterns in synergid cells in response to 0.5 μM and 2 μM RALF19 or RALF34 for WT (**a**), *fer-4* (**b**), *lre-5* (**c**) and *nta-3* (**d**). Red triangles indicate time points at which RALFs was applied.

In Fig 1i, for water treatment, n=13 ovules for WT, n=11 ovules for *fer-4*, n=11 ovules for *lre-5*, and n=11 ovules for *nta-3*; for pollen tube, n=13 ovules for WT, n=17 ovules for *fer-4*, n=7 ovules for *lre-5* and n=10 ovules for *nta-3*; for 0.5 μM RALF4 treatment, n=12 ovules for WT, n=15 ovules for *fer-4*, n=13 ovules for *lre-5* and n=13 ovules for *nta-3*; For 2 μM RALF4 treatment, n=11 ovules for WT, n=10 ovules for *fer-4*, n=13 ovules for *lre-5* and n=14 ovules for *nta-3*; For 0.5 μM RALF19 treatment, n=13 ovules for WT, n=10 ovules *fer-4*, n=11 ovules for *lre-5* and n=12 ovules *nta-3*. For 2 μM RALF19 treatment, n=11 ovules for WT, n=10 ovules for *fer-4*, n=12 ovules for *lre-5* and n=14 ovules for *nta-3*; For

0.5 μM RALF34 treatment, n=11 ovules for WT, n=12 ovules for *fer-4*, n=12 ovules for *lre-5* and n=13 ovules for *nta-3*; For 2 μM RALF34 treatment, n=10 ovules for WT, n=11 ovules for *fer-4*, n=12 ovules for *lre-5* and n=14 ovules for *nta-3*.
In Fig 4k, in WT n=14 ovules for water treatment, n=15 ovules for pollen tube and n=10 ovules for 0.5 μM RALF4 treatment; in *nta-3*, n=11 ovules for water treatment, n=10 ovules for pollen tube and n=12 ovules 0.5 μM RALF4; in NTA^{RR}, n=13 ovules for water treatment, n=14 ovules for pollen tube and n=13 ovules for 0.5 μM RALF4.

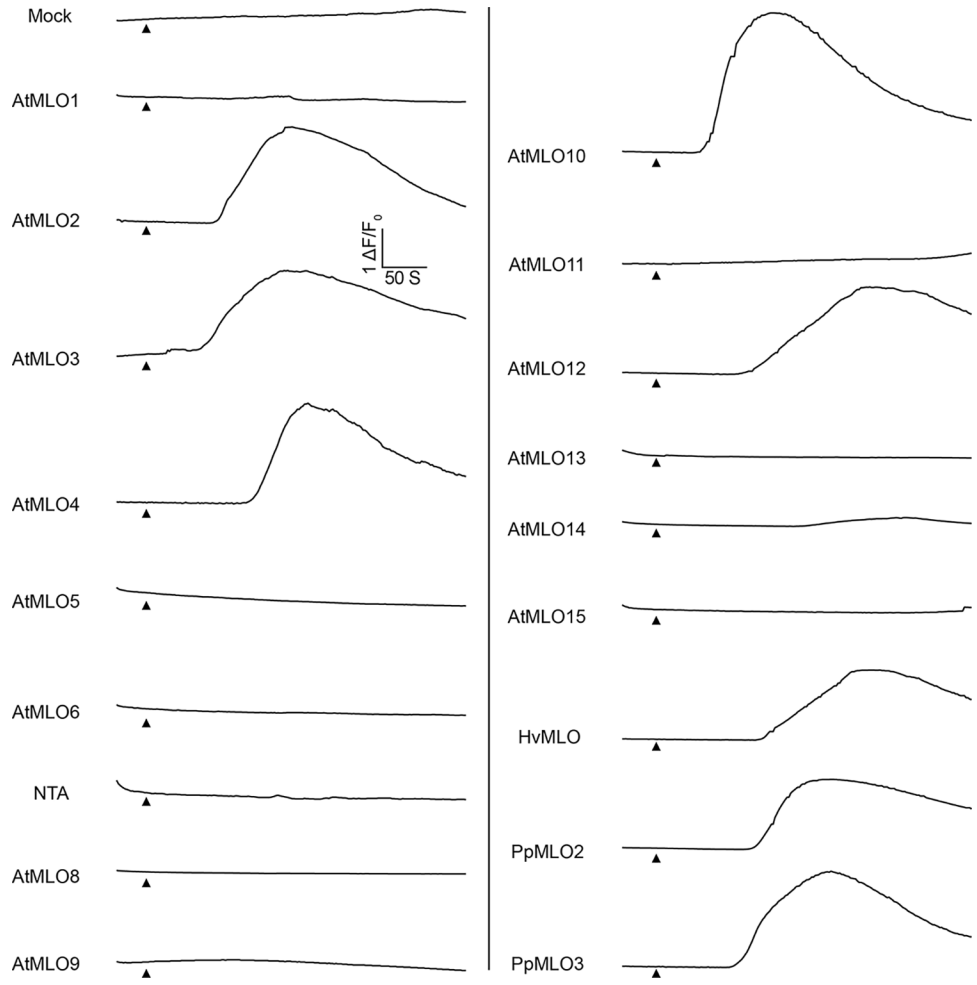

Extended Data Fig.4 |. Representative cytosolic Ca^{2+} increase curves of COS7 cells expressing various MLOs.
The black triangle indicated the time point when 10 mM external Ca^{2+} was applied.

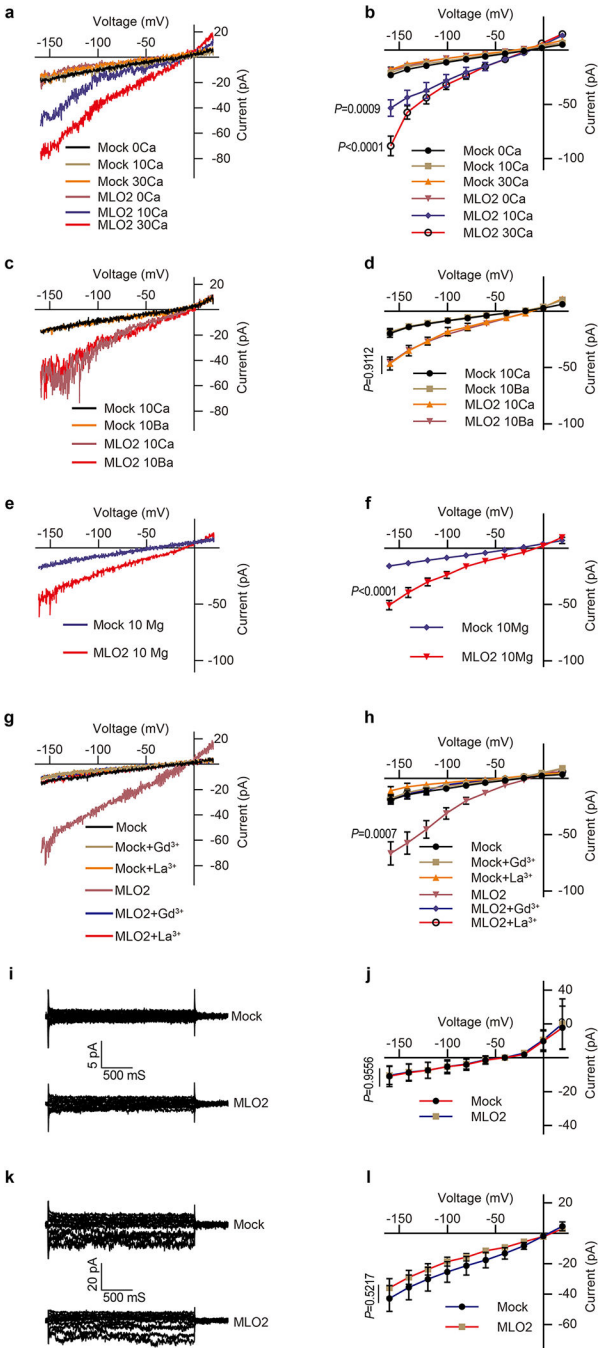

Extended Data Fig.5 |. Conductivity of *At*MLO2 to divalent and monovalent cations.

(**a**) Typical whole-cell recordings and (**b**) average current-voltage curves of the inward currents showing external Ca^{2+} dependence (0 mM, 10 mM and 30mM) in HEK293T cells expressing *At*MLO2. (**c**) Typical whole-cell recordings and (**d**) average current-voltage curves for Ba^{2+} conductance by *At*MLO2 in HEK293T cells. (**e**) Typical whole-cell recordings and (**f**) average current-voltage curves for Mg^{2+} conductance by *At*MLO2 in HEK293T cells. (**g**) Typical whole-cell recordings and (**h**) average current-voltage curves for Gd^{3+} (100 μM) and La^{3+} (100 μM) inhibition of Ca^{2+} conductance in HEK293T

cells expressing *At*MLO2. (**i**) Typical whole-cell recordings and (**j**) average current-voltage curves of the inward currents showing no detectable K^+ conductance by *At*MLO2 in HEK293T cells. (**k**) Typical whole-cell recordings and (**l**) average current-voltage curves of the inward currents showing no detectable Na^+ conductance by *At*MLO2 in HEK293T cells. Error bars depict means ± S.E.M. n values=8 cells. All *P* values were determined by two-tailed Student's *t*-test.

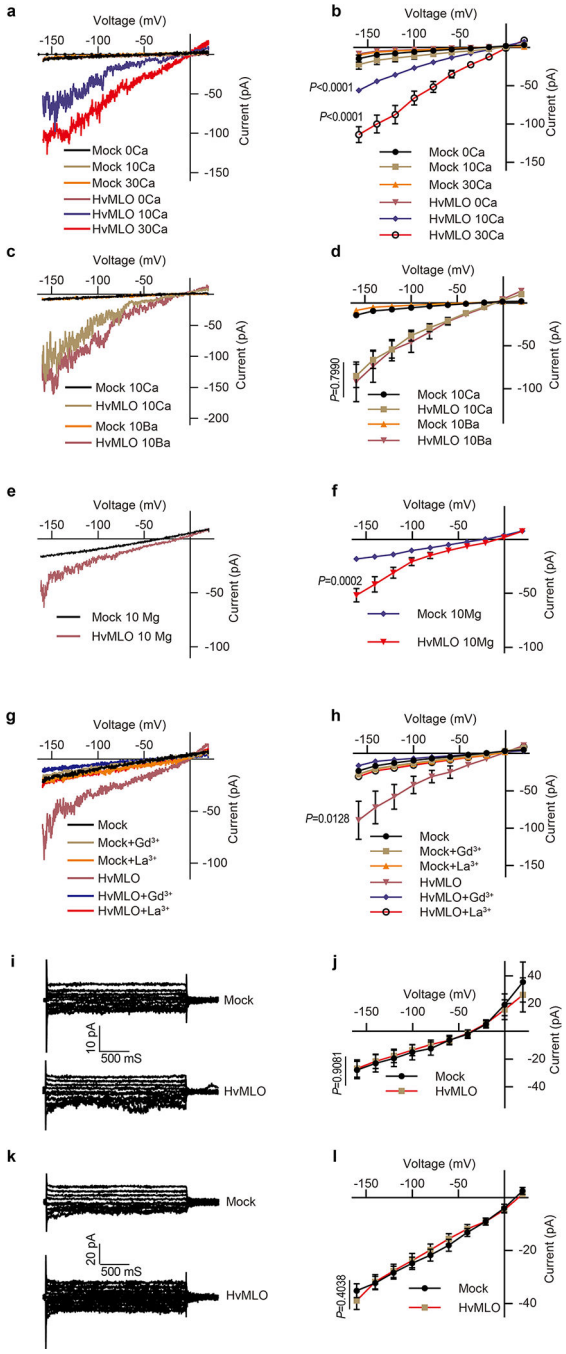

Extended Data Fig.6 |. Conductivity of *Hv*MLO to divalent and monovalent cations.

(**a**) Typical whole-cell recordings and (**b**) average current-voltage curves of the inward currents showing external Ca^{2+} dependence (0 mM, 10 mM and 30mM) in HEK293T cells expressing *Hv*MLO. (**c**) Typical whole-cell recordings and (**d**) average current-voltage curves for Ba^{2+} conductance by *Hv*MLO in HEK293T cells. (**e**) Typical whole-cell recordings and (**f**) average current-voltage curves for Mg^{2+} conductance by *Hv*MLO in HEK293T cells. (**g**) Typical whole-cell recordings and (**h**) average current-voltage curves for Gd^{3+} (100 μM) and La^{3+} (100 μM) inhibition of Ca^{2+} conductance in HEK293T cells expressing *Hv*MLO. (**i**) Typical whole-cell recordings and (**j**) average current-voltage curves of the inward currents showing no detectable K^+ conductance by *Hv*MLO in HEK293T cells. (**k**) Typical whole-cell recordings and (**l**) average current-voltage curves of the inward currents showing no detectable Na^+ conductance by *Hv*MLO in HEK293T cells. Error bars depict means ± S.E.M. n values=8 cells. All *P* values were determined by two-tailed Student's *t*-test.

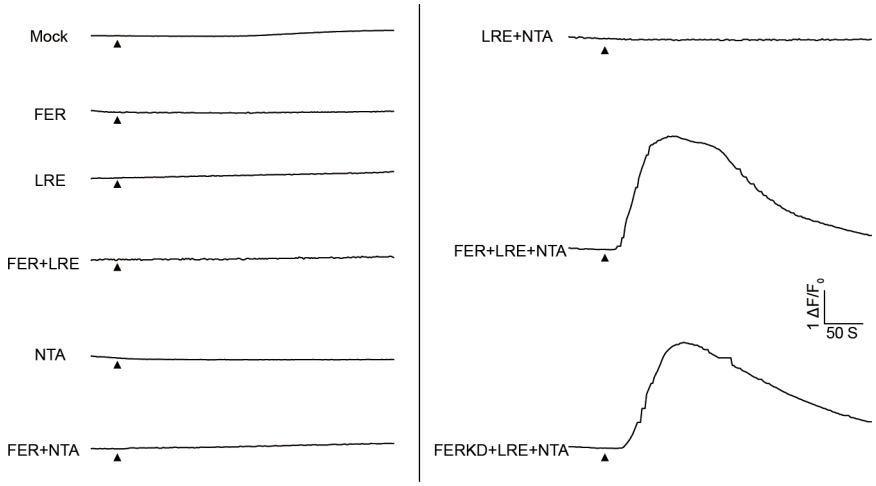

Extended Data Fig.7 |. Typical cytosolic Ca^{2+} increase curves of COS7 cells expressing the combination of FER, LRE, NTA and the kinase-dead version of FER (FERKD).
The black triangle indicated the time point when 10 mM external Ca^{2+} was applied.

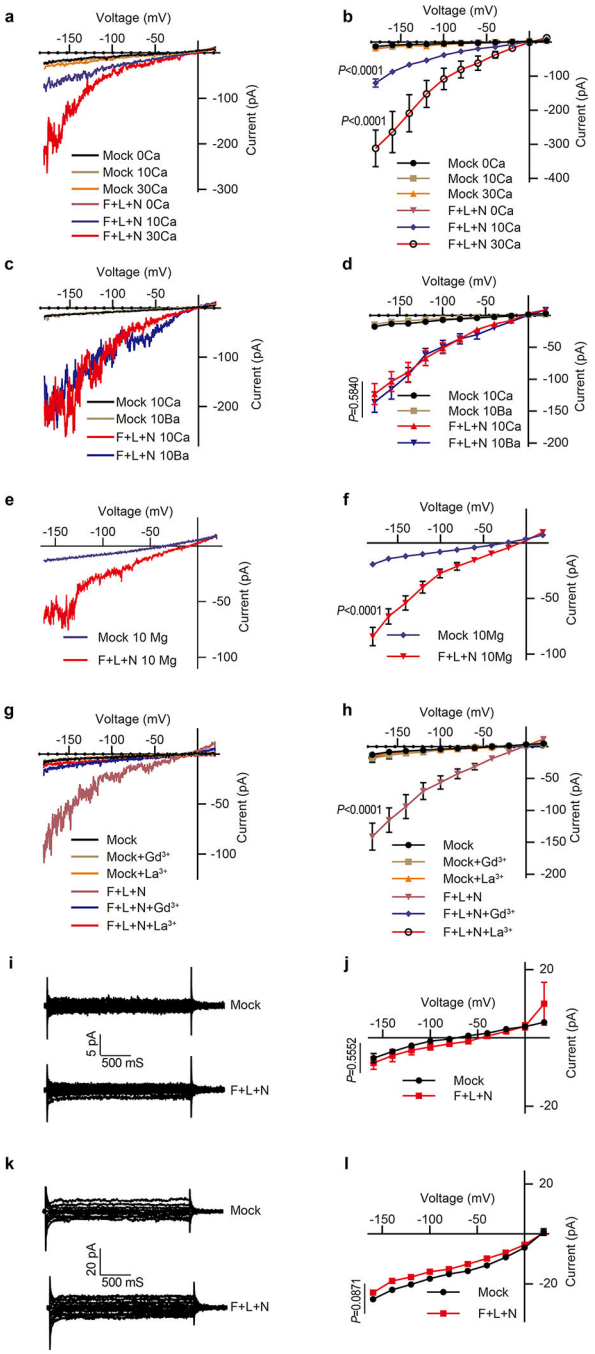

Extended Data Fig.8 |. Conductivity of NTA trio to divalent and monovalent cations.

(**a**) Typical whole-cell recordings and (**b**) average current-voltage curves of the inward currents showing external Ca^{2+} dependence (0 mM, 10 mM and 30mM) in HEK293T cells expressing NTA trio. (**c**) Typical whole-cell recordings and (**d**) average current-voltage curves for Ba^{2+} conductance by NTA trio in HEK293T cells. (**e**) Typical whole-cell recordings and (**f**) average current-voltage curves for Mg^{2+} conductance by NTA trio in HEK293T cells. (**g**) Typical whole-cell recordings and (**h**) average current-voltage curves for Gd^{3+} (100 μM) and La^{3+} (100 μM) inhibition of Ca^{2+} conductance in HEK293T cells

expressing NTA trio. (**i**) Typical whole-cell recordings and (**j**) average current-voltage curves of the inward currents showing no detectable K^+ conductance by NTA trio in HEK293T cells. (**k**) Typical whole-cell recordings and (**l**) average current-voltage curves of the inward currents showing no detectable Na^+ conductance by NTA trio in HEK293T cells. Error bars depict means ± S.E.M. n values=8 cells. All *P* values were determined by two-tailed Student's *t*-test.

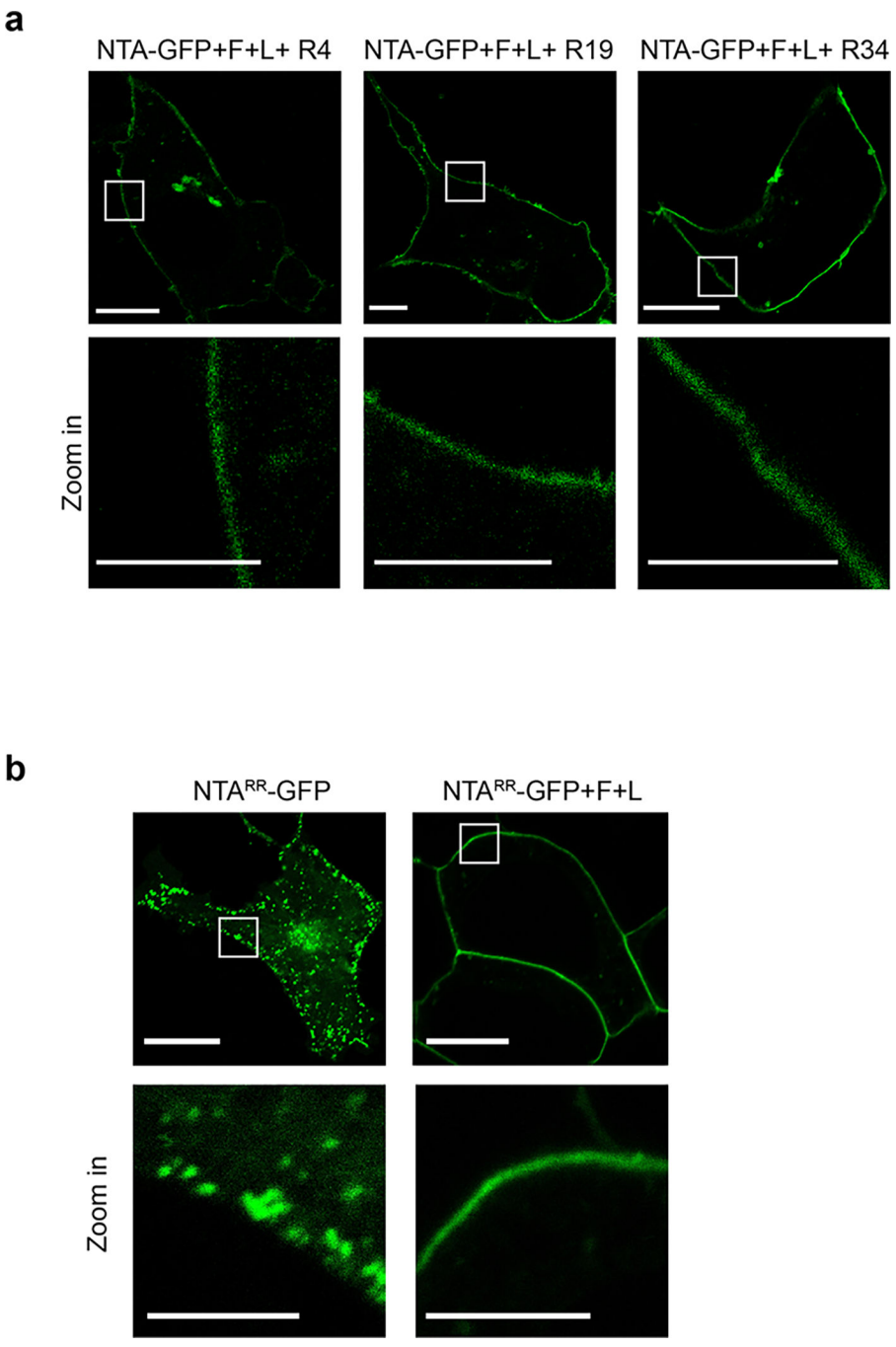

Extended Data Fig.9 |. The localization of NTA-GFP and NTA^{RR}-GFP.

a, RALFs did not alter the PM localization of NTA-GFP. n=3 independent repeats. **b**, FER and LRE facilitated the PM localization of NTA^{RR}-GFP. Scale bars, 10 μm (up-panel), 5 μm (down-panel). The white rectangle indicated the area of zoom-in. n=3 independent repeats.

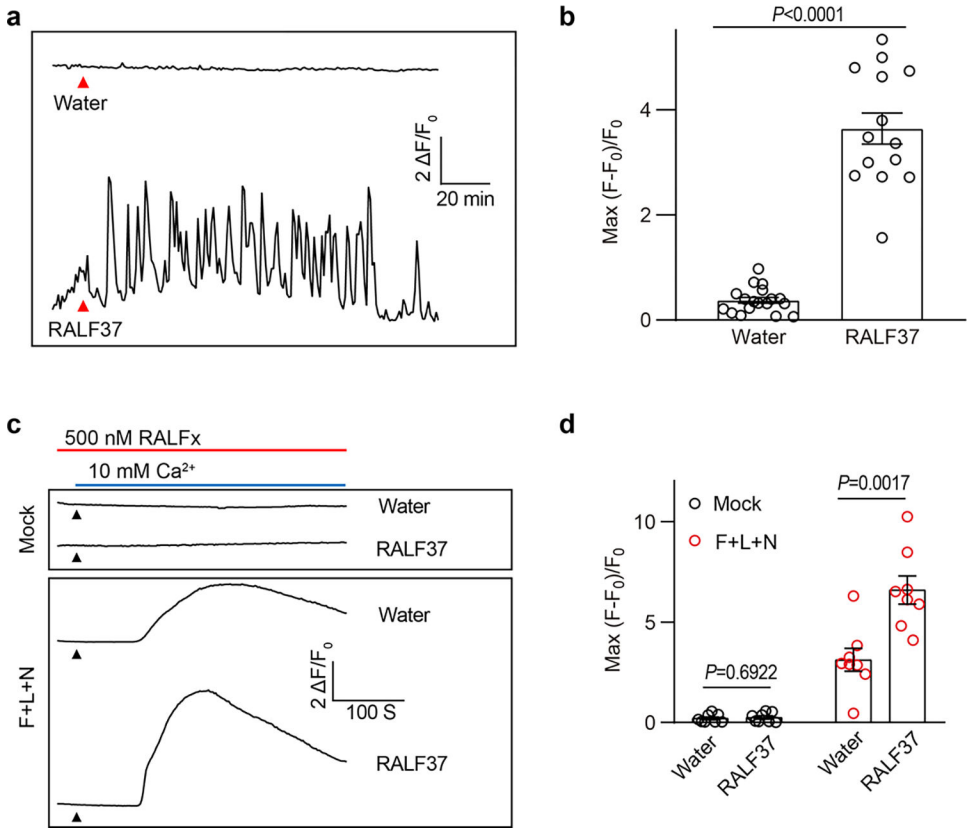

Extended Data Fig.10 |. RALF37 triggers synergid Ca^{2+} changes and enhances the activity of NTA trio.

a, Representative Ca^{2+} spiking patterns in synergid cells in response to 0.5 μM RALF37. **b**, The peak values of Ca^{2+} spiking as in (**a**). n=18 ovules for water treatment and n=14 ovules for RALF37. **c**, **d**, Representative cytosolic Ca^{2+} spiking curves (**c**) and statistical analysis of peak values (**d**) in COS7 cells expressing the FER-LRE-NTA trio treated with 0.5 μM RALF37. n = 8 replicates, and ~ 60 cells were imaged in each duplicate. Error bars depict means ± S.E.M. All *P* values were determined by two-tailed Student's *t*-test.

Supplementary Material

Refer to Web version on PubMed Central for supplementary material.

Acknowledgments:

We thank Julia Santiago of University of Lausanne for providing the pFastBac-RALF4/19 and LRX8 vector, and Baobin Li of UC Berkeley for advice on protein purification from insect cells. We also thank Ravishankar Palanivelu of University of Arizona for providing p*LAT52*: DsRed seeds. We appreciate assistance from Steven Ruzin and Denise Schichnes in The Biological Imaging Facility of UC Berkeley.

Data availability

The data supporting the findings of this study are available within the paper and its Supplementary Information files. Source Data for Figs. 1–4 and Extended Data Figs. 1–10 are provided with the paper.

References

1. Johnson MA, Harper JF & Palanivelu R A fruitful journey: pollen tube navigation from germination to fertilization. Annu Rev Plant Biol 70, 809–837 (2019). [PubMed: 30822112]
2. Denninger P et al. Male-female communication triggers calcium signatures during fertilization in *Arabidopsis*. Nat Commun 5, 4645 (2014). [PubMed: 25145880]
3. Ngo QA, Vogler H, Lituiev DS, Nestorova A & Grossniklaus U A calcium dialog mediated by the FERONIA signal transduction pathway controls plant sperm delivery. Dev Cell 29, 491–500 (2014). [PubMed: 24814317]
4. Escobar-Restrepo JM et al. The FERONIA receptor-like kinase mediates male-female interactions during pollen tube reception. Science 317, 656–660 (2007). [PubMed: 17673660]
5. Liu X et al. The role of LORELEI in pollen tube reception at the interface of the synergid cell and pollen tube requires the modified eight-cysteine motif and the receptor-like kinase FERONIA. Plant Cell 28, 1035–1052 (2016). [PubMed: 27081182]
6. Kessler SA et al. Conserved molecular components for pollen tube reception and fungal invasion. Science 330, 968–971 (2010). [PubMed: 21071669]
7. Ge Z et al. *Arabidopsis* pollen tube integrity and sperm release are regulated by RALF-mediated signaling. Science 358, 1596–1600 (2017). [PubMed: 29242234]
8. Blackburn MR, Haruta M & Moura DS Twenty years of progress in physiological and biochemical investigation of RALF peptides. Plant Physiol 182, 1657–1666 (2020). [PubMed: 32071151]
9. Clapham DE Calcium signaling. Cell 131, 1047–1058 (2007). [PubMed: 18083096]
10. Trewavas A Le calcium, C'est la vie: calcium makes waves. Plant Physiol 120, 1–6 (1999). [PubMed: 10318677]
11. Luan S & Wang C Calcium signaling mechanisms across kingdoms. Annu Rev Cell Dev Biol 37, 311–340 (2021). [PubMed: 34375534]
12. Hwang JY et al. Dual sensing of physiologic pH and calcium by EFCAB9 regulates sperm motility. Cell 177, 1480–1494 e1419 (2019). [PubMed: 31056283]
13. Whitaker M Calcium at fertilization and in early development. Physiological reviews 86, 25–88 (2006). [PubMed: 16371595]
14. Chen J, Gutjahr C, Bleckmann A & Dresselhaus T Calcium signaling during reproduction and biotrophic fungal interactions in plants. Mol Plant 8, 595–611 (2015). [PubMed: 25660409]
15. Hamamura Y et al. Live imaging of calcium spikes during double fertilization in *Arabidopsis*. Nat Commun 5, 4722 (2014). [PubMed: 25146889]
16. Iwano M et al. Cytoplasmic Ca^{2+} changes dynamically during the interaction of the pollen tube with synergid cells. Development 139, 4202–4209 (2012). [PubMed: 23093426]
17. Ge Z, Dresselhaus T & Qu LJ How CrRLK1L receptor complexes perceive RALF signals. Trends Plant Sci 24, 978–981 (2019). [PubMed: 31607472]
18. Franck CM, Westermann J & Boisson-Dernier A Plant malectin-like receptor kinases: from cell wall integrity to immunity and beyond. Annu Rev Plant Biol 69, 301–328 (2018). [PubMed: 29539271]
19. Li C et al. Glycosylphosphatidylinositol-anchored proteins as chaperones and co-receptors for FERONIA receptor kinase signaling in *Arabidopsis*. Elife 4 (2015).
20. Cheung AY, Qu LJ, Russinova E, Zhao Y & Zipfel C Update on receptors and signaling. Plant Physiol 182, 1527–1530 (2020). [PubMed: 32253323]
21. Haruta M, Sabat G, Stecker K, Minkoff BB & Sussman MR A peptide hormone and its receptor protein kinase regulate plant cell expansion. Science 343, 408–411 (2014). [PubMed: 24458638]

22. Stegmann M et al. The receptor kinase FER is a RALF-regulated scaffold controlling plant immune signaling. Science 355, 287–289 (2017). [PubMed: 28104890]
23. Xiao Y et al. Mechanisms of RALF peptide perception by a heterotypic receptor complex. Nature 572, 270–274 (2019). [PubMed: 31291642]
24. Ge Z et al. LLG2/3 are co-receptors in BUPS/ANX-RALF signaling to regulate *Arabidopsis* pollen tube integrity. Curr Biol 29, 3256–3265 e3255 (2019). [PubMed: 31564495]
25. Liu C et al. Pollen PCP-B peptides unlock a stigma peptide-receptor kinase gating mechanism for pollination. Science 372, 171–175 (2021). [PubMed: 33833120]
26. Zhou X et al. Membrane receptor-mediated mechano-transduction maintains cell integrity during pollen tube growth within the pistil. Dev Cell 56, 1030–1042 e1036 (2021). [PubMed: 33756107]
27. Liu KH et al. Discovery of nitrate-CPK-NLP signalling in central nutrient-growth networks. Nature 545, 311–316 (2017). [PubMed: 28489820]
28. Kasahara RD, Portereiko MF, Sandaklie-Nikolova L, Rabiger DS & Drews GN MYB98 is required for pollen tube guidance and synergid cell differentiation in *Arabidopsis*. Plant Cell 17, 2981–2992 (2005). [PubMed: 16214903]
29. Buschges R et al. The barley Mlo gene: a novel control element of plant pathogen resistance. Cell 88, 695–705 (1997). [PubMed: 9054509]
30. Devoto A et al. Molecular phylogeny and evolution of the plant-specific seven-transmembrane MLO family. J Mol Evol 56, 77–88 (2003). [PubMed: 12569425]
31. Kusch S, Pesch L & Panstruga R Comprehensive phylogenetic analysis sheds light on the diversity and origin of the MLO family of integral membrane proteins. Genome Biol Evol 8, 878–895 (2016). [PubMed: 26893454]
32. Chen Z et al. Two seven-transmembrane domain MILDEW RESISTANCE LOCUS O proteins cofunction in *Arabidopsis* root thigmomorphogenesis. Plant Cell 21, 1972–1991 (2009). [PubMed: 19602625]
33. Consonni C et al. Conserved requirement for a plant host cell protein in powdery mildew pathogenesis. Nat Genet 38, 716–720 (2006). [PubMed: 16732289]
34. Meng JG et al. Integration of ovular signals and exocytosis of a Ca^{2+} channel by MLOs in pollen tube guidance. Nat Plants 6, 143–153 (2020). [PubMed: 32055051]
35. Pan Y et al. Dynamic interactions of plant CNGC subunits and calmodulins drive oscillatory Ca^{2+} channel activities. Dev Cell 48, 710–725 e715 (2019). [PubMed: 30713075]
36. Jones DS et al. MILDEW RESISTANCE LOCUS O function in pollen tube reception is linked to its oligomerization and subcellular distribution. Plant Physiol 175, 172–185 (2017). [PubMed: 28724621]
37. Ju Y et al. Polarized NORTIA accumulation in response to pollen tube arrival at synergids promotes fertilization. Dev Cell 56, 2938–2951 e2936 (2021). [PubMed: 34672969]
38. Kessler SA, Lindner H, Jones DS & Grossniklaus U Functional analysis of related CrRLK1L receptor-like kinases in pollen tube reception. EMBO Rep 16, 107–115 (2015). [PubMed: 25490905]
39. Haruta M, Gaddameedi V, Burch H, Fernandez D & Sussman MR Comparison of the effects of a kinase-dead mutation of FERONIA on ovule fertilization and root growth of *Arabidopsis*. FEBS Lett 592, 2395–2402 (2018). [PubMed: 29904923]
40. Zhong S et al. RALF peptide signaling controls the polytubey block in *Arabidopsis*. Science 375, 290–296 (2022). [PubMed: 35050671]
41. Ben-Johny M & Yue DT Calmodulin regulation (calmodulation) of voltage-gated calcium channels. J Gen Physiol 143, 679–692 (2014). [PubMed: 24863929]
42. Tian W, Wang C, Gao Q, Li L & Luan S Calcium spikes, waves and oscillations in plant development and biotic interactions. Nat Plants 6, 750–759 (2020). [PubMed: 32601423]
43. Kim MC et al. Calmodulin interacts with MLO protein to regulate defence against mildew in barley. Nature 416, 447–451 (2002). [PubMed: 11919636]
44. Tian W et al. A calmodulin-gated calcium channel links pathogen patterns to plant immunity. Nature 572, 131–135 (2019). [PubMed: 31316205]

45. Clough SJ, Bent AF Floral dip: a simplified method for *Agrobacterium*-mediated transformation of *Arabidopsis thaliana*. Plant J 16, 735–743 (1998). [PubMed: 10069079]

46. Gao QF et al. Cyclic nucleotide-gated channel 18 is an essential Ca^{2+} channel in pollen tube tips for pollen tube guidance to ovules in *Arabidopsis*. Proc Natl Acad Sci U S A 113, 3096–3101 (2016). [PubMed: 26929345]

47. Palanivelu R, Preuss D Distinct short-range ovule signals attract or repel *Arabidopsis thaliana* pollen tubes in vitro. BMC Plant Biol 6, 7 (2006). [PubMed: 16595022]

48. Li H et al. Control of pollen tube tip growth by a Rop GTPase-dependent pathway that leads to tip-localized calcium influx. Plant Cell 11, 1731–1742 (1999). [PubMed: 10488239]

49. Moussu S et al. Structural basis for recognition of RALF peptides by LRX proteins during pollen tube growth. Proc Natl Acad Sci U S A 117, 7494–7503 (2020). [PubMed: 32165538]

50. Duan Q et al. FERONIA receptor-like kinase regulates RHO GTPase signaling of root hair development. Proc Natl Acad Sci U S A 107, 17821–17826 (2010). [PubMed: 20876100]

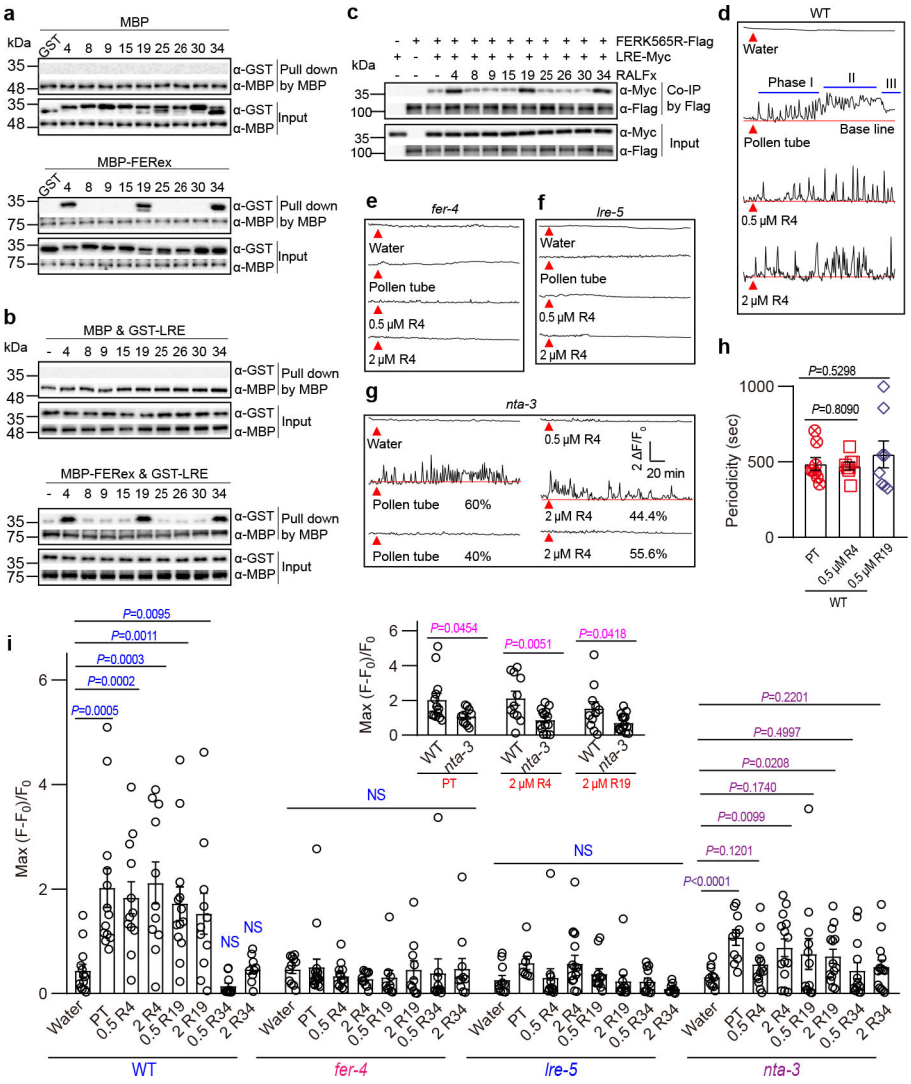

Fig. 1 |. Pollen-derived RALFs bind to FER-LRE and trigger synergid $[Ca^{2+}]_{cyt}$ changes in a FER-LRE-NTA-dependent manner.

a, Pull-down assays showing interaction of GST-tagged RALFs and MBP-tagged ectodomains of FER (FER_{ex}). Amylose resin was used to pull-down MBP, followed by western blots with antibodies against GST (α-GST) and MBP (α-MBP). n=3 independent repeats. **b**, Interaction of GST-tagged LRE and MBP-tagged ectodomains of FER with or without RALFs (each 100 nM) as indicated. Amylose resin pull-down and western was performed as in (**a**). n=3 independent repeats. **c**, Co-IP of Myc-tagged LRE and Flag-tagged FERK565R expressed in *Nicotiana benthamiana* leaves with or without addition of RALFs (each 5 μM) as indicated. Anti-Flag M2 affinity bead was used in co-IP, and western blots were probed with antibodies against Myc (α-Myc) and Flag (α-Flag). n=3 independent repeats. **d-7g**, Representative Ca^{2+} spiking patterns in synergid cells in response to pollen tube arrival (PT) or 0.5 μM/2 μM RALF4 (R4) for WT (**d**), *fer-4* (**e**), *lre-5* (**f**) and *nta-3* (**g**). (**h**) Ca^{2+} oscillation periodicity of WT synergids in response to pollen tube arrival or 0.5 μM RALF4/19. n = 8 ovules. **i**, The peak values of Ca^{2+} spiking as in (**d** to **g**). n values were shown in Extended Data Fig. 3. Ovules were isolated from Col-0, *fer-4*, *lre-5* and

nta-3 flowers harboring the synergid-specific GCaMP6 and fluorescence was recorded by an inverted microscope. Red triangles indicate time points at which pollen tube arrived or 0.5 μM RALF4 was applied. Error bars depict means ± S.E.M. All *P* values were determined by two-tailed Student's *t*-test. NS, not significant.

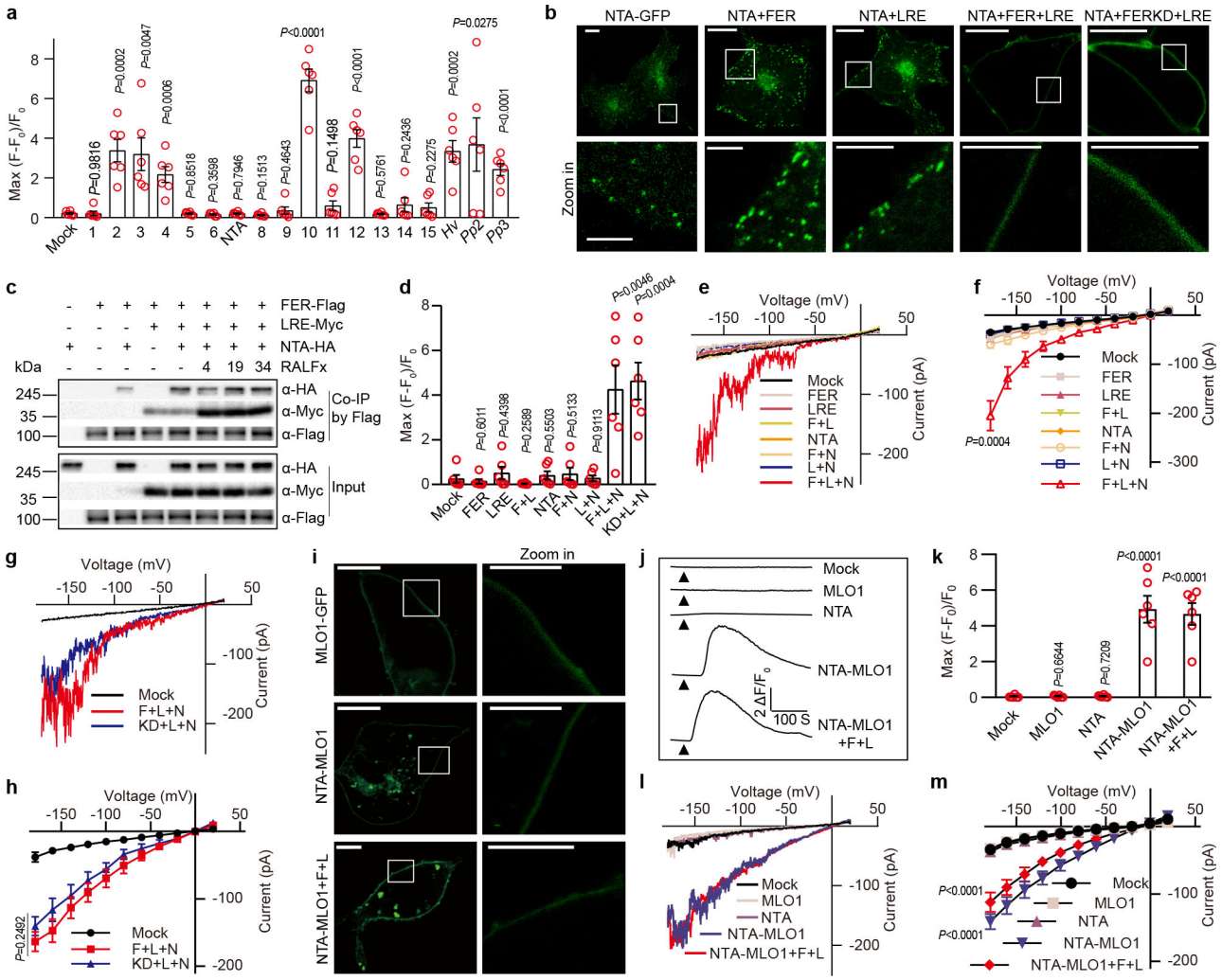

Fig. 2 |. MLO family proteins, including NTA, are Ca^{2+} permeable channels.

a, $[Ca^{2+}]_{cyt}$ elevation measured by single cell fluorescence imaging in HEK293T cells expressing various MLOs. *Hv* denoted *Hv*MLO, *Pp*2 denote *Pp*MLO2, and *Pp*3 denote *Pp*MLO3. **b**, FER and LRE facilitated the PM localization of NTA-GFP. Scale bars, 10 μm (up-panel), 5 μm (down-panel). The white rectangle indicated the area magnified in the lower panel. n=3 independent repeats. **c**, Co-IP of HA-tagged NTA, Myc-tagged LRE and Flag-tagged FER expressed in *Xenopus* oocytes with or without the addition of RALFs (each 5 μM) as indicated. Anti-Flag M2 affinity bead was used to co-IP, and western blots were probed with antibodies against Myc (α-Myc), HA (α-HA) and Flag (α-Flag). n=3 independent repeats. **d**, $[Ca^{2+}]_{cyt}$ elevation measured by single cell imaging of in HEK293T cells expressing NTA (N), FER (F), FERK565R (kinase dead version) (KD) and LRE (L). (**e-f**) Typical whole-cell recordings (**e**) and current-voltage curves (**f**) of inward currents in HEK293T cells expressing NTA, FER and LRE. Similar analyses were conducted for HEK293T cells expressing NTA, LRE and the kinase-dead version of FER (**g-h**). **i**, MLO1 C-terminal cytosolic tail facilitated the PM localization of NTA-GFP. NTA-MLO1 denoted the chimeric protein of NTA and MLO1 C terminal tail. Scale bars, 10 μm (left-panel), 5 μm (right-panel). n=3 independent repeats. (**j-k**) Representative cytosolic Ca^{2+} spiking curves

(**j**) and statistical analysis of peak values (**k**) in COS7 cells expressing the NTA-MLO1 chimeric or original channels. (**l-m**) Typical whole-cell recordings (**l**) and current-voltage curves (**m**) of inward currents in HEK293T cells expressing the NTA-MLO1 chimeric or original channels. For Ca^{2+} imaging in HEK293T cells, n =6 replicates, and ~ 60 cells were imaged in each duplicate. For patch-clamp, n=8 cells. Error bars depict means ± S.E.M. All *P* values were determined by two-tailed Student's *t*-test.

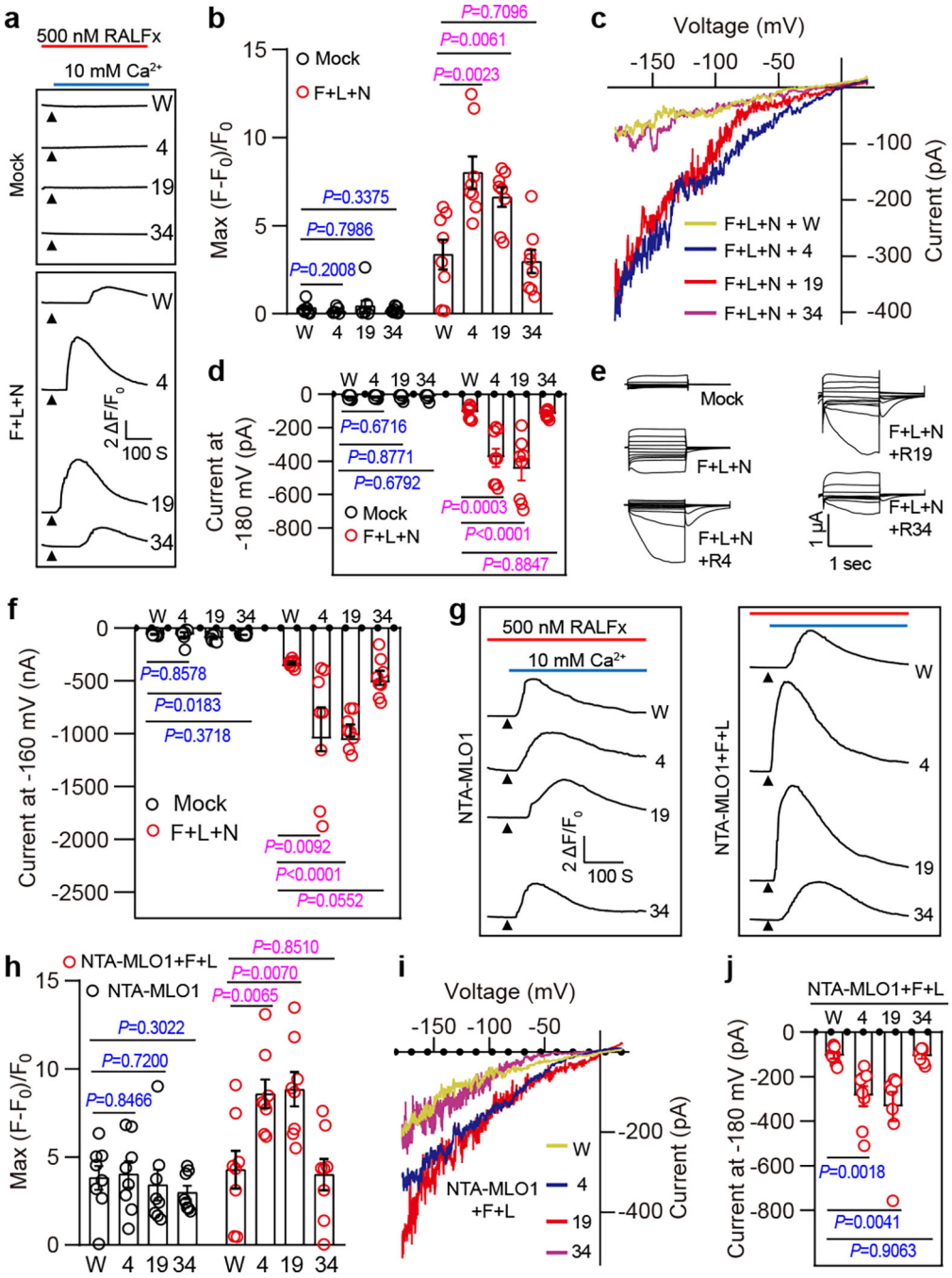

Fig. 3 |. RALFs enhance the Ca^{2+} channel activity of FER-LRE-NTA trio.

a, **b**, Representative cytosolic Ca^{2+} spiking curves (**a**) and statistical analysis of peak values (**b**) in COS7 cells expressing FER-LRE-NTA trio or mock cells treated with various RALFs. The arrowheads indicate the time points at which 10 mM Ca^{2+} was applied. W denoted water, 4 denoted RALF4, 19 denoted RALF19, and 34 denoted RALF34. **c**, **d**, Typical whole-cell recording traces using ramping protocol (**c**) and amplitudes at −180 mV (**d**) of Ca^{2+}-permeable inward currents in HEK293T cells expressing FER-LRE-NTA trio or mock cells treated with various RALFs. **e**, **f**, Typical TEVC recordings (**e**) and current amplitudes

at −160 mV (**f**) of inward currents in *Xenopus* oocytes expressing FER-LRE-NTA trio or mock water-injected oocytes treated with various RALFs. **g**, **h**, Representative cytosolic Ca^{2+} spiking curves (**g**) and statistical analysis of peak values (**h**) in COS7 cells expressing the chimeric NTA-MLO1 or FER-LRE-NTA-MLO1 trio cells treated with various RALFs. **i**, **j**, Typical whole-cell recording traces using ramping protocol (**i**) and amplitudes at −180 mV (**j**) of Ca^{2+}-permeable inward currents in HEK293T cells expressing FER-LRE-NTA-MLO1 trio treated with various RALFs. For Ca^{2+} imaging in HEK293T cells, n =8 replicates, and ~ 60 cells were imaged in each duplicate. For HEK293T cell recording, n=8 cells. For oocyte recording, n=8 oocytes. Error bars depict means ± S.E.M. All *P* values were determined by two-tailed Student's *t*-test.

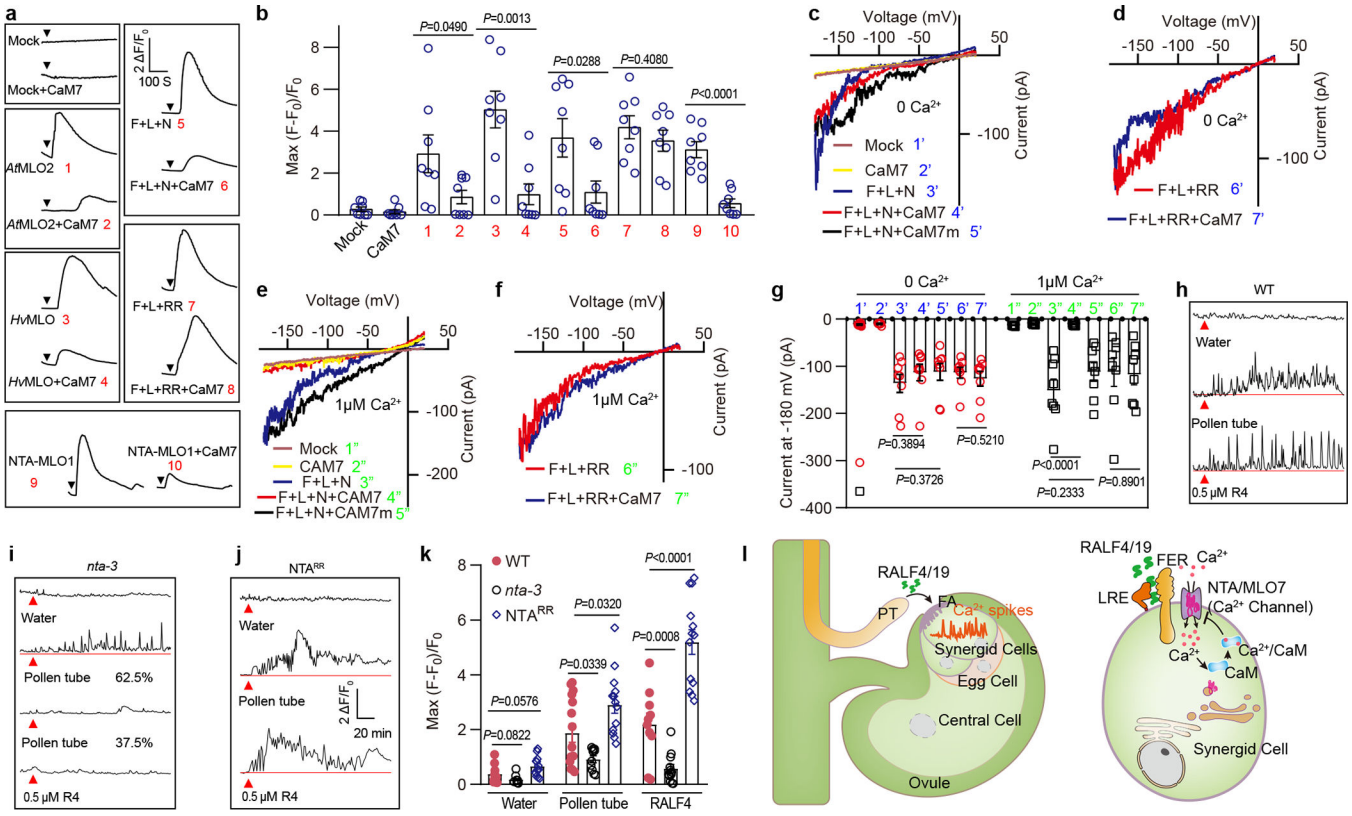

Fig. 4 |. Calmodulin inhibition of NTA Ca^{2+} channel is involved in modeling Ca^{2+}-spiking pattern in synergid.

a, **b**, Typical Ca^{2+} spiking patterns (**a**) and peak values (**b**) in COS7 cells expressing MLOs and *At*CaM7. The arrowheads indicate the time points at which 10 mM external Ca^{2+} was applied. n = 8 replicates, and ~ 60 cells were imaged in each duplicate. **c-f** Typical whole-cell recordings of inward currents in HEK293T cells expressing NTA trio, *At*CaM7 or mock cells when $[Ca^{2+}]_{cyt}$ was 0 nM (**c**, **e**) or 1 μM (**d**, **f**). **g**, Current amplitudes at −180 mV of HEK293T cells expressing NTA trio and *At*CaM7 when $[Ca^{2+}]_{cyt}$ was 0 nM or 1 μM. n=8 cells. **h- j**, Representative Ca^{2+} spiking patterns in synergid cells in response to pollen tube arrival (PT) or 0.5 μM RALF4 (R4) for WT (**h**), *nta-3* (**i**) and NTA^{RR} (**j**). **k**, The peak values of Ca^{2+} spiking as in (**h** to **j**). n values were shown in Extended Data Fig. 3. Error bars depict means ± S.E.M. All *P* values were determined by two-tailed Student's *t*-test. **l**, Model of RALF-FER/LRE-NTA pathway leading to synergid Ca^{2+} changes. Upon pollen tube arrival, pollen tube-derived RALF4/19 bind FER/LRE that recruit and activate the NTA, a CaM-gated calcium channel, to initiate calcium spiking.